



LAWRENCE  
LIVERMORE  
NATIONAL  
LABORATORY

# Measurement of the dispersion of thermal ion-acoustic fluctuations in high-temperature laser plasmas using multiple wavelength Thomson-scattering

D. H. Froula, P. Davis, L. Divol, J. S. Ross, N. Meezan,  
D. Price, S. H. Glenzer, C. Rousseaux

June 6, 2005

Physics Review Letters

## **Disclaimer**

---

This document was prepared as an account of work sponsored by an agency of the United States Government. Neither the United States Government nor the University of California nor any of their employees, makes any warranty, express or implied, or assumes any legal liability or responsibility for the accuracy, completeness, or usefulness of any information, apparatus, product, or process disclosed, or represents that its use would not infringe privately owned rights. Reference herein to any specific commercial product, process, or service by trade name, trademark, manufacturer, or otherwise, does not necessarily constitute or imply its endorsement, recommendation, or favoring by the United States Government or the University of California. The views and opinions of authors expressed herein do not necessarily state or reflect those of the United States Government or the University of California, and shall not be used for advertising or product endorsement purposes.

# Measurement of the dispersion of thermal ion-acoustic fluctuations in high-temperature laser plasmas using multiple wavelength Thomson-scattering

D. H. Froula,\* P. Davis,† L. Divol, J. S. Ross,‡ N. Meezan, D. Price, and S. H. Glenzer  
*L-399, Lawrence Livermore National Laboratory, P.O. Box 808, Livermore, CA 94551, USA*

C. Rousseaux

*CEA-DIF, Centre de Bruyres-le-Chitel, B.P. 12, 91680 Bruyres-le-Chitel, France*

(Dated: May 12, 2005)

The dispersion of ion-acoustic fluctuations has been measured using a novel technique that employed multiple color Thomson scattering to measure the frequency spectrum for two separate thermal ion-acoustic fluctuations with significantly different wave vectors. The plasma fluctuations are shown to become dispersive with increasing electron temperature. We demonstrate that this technique allows a time resolved local measurement of electron density and temperature in inertial confinement fusion plasmas.

PACS numbers: 52.25.Os, 52.35.Fp, 52.50.Jm

Keywords: ion-acoustic wave, dispersion, Thomson scattering

Thermal density fluctuations in a plasma result from the finite motion of the electrons and ions. Experiments over the last forty years have used Thomson scattering to extract fundamental plasma properties from the frequency spectrum and is now widely used in Magnetic Fusion (MFE) and Inertial Confinement Fusion (ICF). Thomson scattering can directly measure the frequency spectrum of the density fluctuations for a given wave vector; the incident laser light ( $k_o, \omega_o$ ) is Doppler shifted when scattered by the finite motion of the electrons. For collective Thomson scattering ( $\frac{ZT_e}{T_i} \gg k_a^2 \lambda_{De}^2$ ), the frequency of the scattered light is up-shifted and down-shifted from the laser frequency. The peak-to-peak wavelength separation ( $\Delta\lambda_{ts}$ ) in the Thomson-scattering spectrum is a direct measure of the ion-acoustic frequency. In ICF, collective Thomson scattering is often used to measure electron temperature by probing the low frequency ion-acoustic fluctuations [?] while, in theory, the electron density can be obtained from the electron plasma wave, it has been a much more challenging measurement in laser produced plasmas [1].

The power spectrum for thermal density fluctuations in a plasma can be expressed using a theoretical form factor [2]:

$$S(k, \omega) = \frac{2\pi}{k} \left| 1 - \frac{\chi_e}{\epsilon} \right|^2 f_e \left( \frac{\omega}{k} \right) + \frac{2\pi Z}{k} \left| 1 - \frac{\chi_i}{\epsilon} \right|^2 f_i \left( \frac{\omega}{k} \right) \quad (1)$$

where  $\epsilon = 1 + \chi_e + \chi_i$  is the plasma dielectric function. For low frequency fluctuations, namely ion-acoustic modes, the phase velocity ( $v_\phi$ ) is in the tail of the ion distribution function ( $f_i(\frac{\omega}{k} \gg v_\phi) \sim 0$ ) and near the peak of the electron distribution function ( $f_e(\frac{\omega}{k} \ll v_\phi) \sim 1$ ), therefore, Eq. 1 is dominated by the first term on the right hand side. The frequency of the resonant fluctuations will therefore be near the point where epsilon approaches zero, although experiments with multi-ion-species plasmas have suggested that this is not always the case [3].

In 1966 [4], low frequency modes that were excited in low temperature plasmas ( $< 1$  eV,  $k\lambda_{De} < 1$ ) were shown to follow the ion-acoustic dispersion relation (i.e.  $\epsilon = 0$ ).

In the fluid limit, solving the dispersion relation ( $\epsilon(\omega, k) = 0$ ) leads to the ion-acoustic sound speed;

$$\frac{\omega_a}{k_a} = \sqrt{\frac{ZT_e}{M(1 + k_a^2 \lambda_{De}^2)} + \frac{3T_i}{M}}. \quad (2)$$

The first term on the right hand side results from electron screening; when the wavelength of the fluctuation is larger than the electron Debye length ( $\lambda_{De} = \sqrt{\epsilon_o T_e / n_e e^2}$ ), the plasma is non-dispersive. When the wavelength of the fluctuation decreases, the electron screening begins to break down and the plasma becomes dispersive; the sound speed of an ion-acoustic wave in a dispersive plasma is dependent on the frequency.

In this paper, we present a novel measure of the dispersion of thermal ion-acoustic fluctuations in a dense high-temperature plasma for a variety of electron densities ( $0.2 < k_a \lambda_{De} < 1.5$ ). The use of Thomson-scattering diagnostics at multiple probe wavelengths allowed us to measure the local frequency of the ion-acoustic fluctuations for two significantly different wave vectors. Figure 1 shows the local frequency measurements and the effects of a dispersive plasma which is a verification of a fundamental property of ion-acoustic fluctuations in a hot inertial confinement plasma. Furthermore, this technique is shown to be a powerful diagnostic of both the local electron density and local electron temperature with high temporal and spatial resolution and could be adapted for a variety of applications across the fields of plasma physics where other diagnostics have not successfully provided accurate local density and temperature measurements.

This experiment used a four laser beam configuration at the recently upgraded Janus Long Pulse Facility at

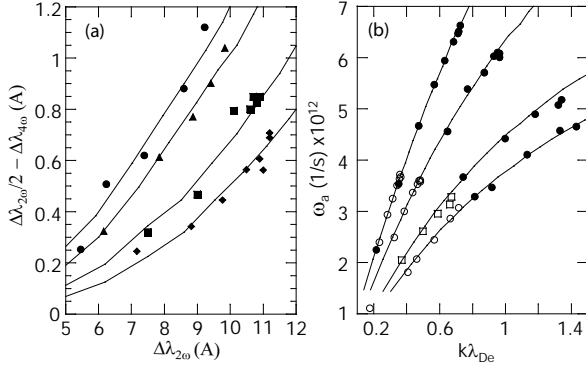


FIG. 1: (a) As the electron temperature increased (increasing  $\Delta\lambda_{2\omega}$ ) or the electron density decreases (each curve represents a single density), the plasma becomes more dispersive; the normalized wavelength difference in a non-dispersive plasma would follow the x-axis. (b) The open/closed circles are the measured ion-acoustic frequencies from the  $2\omega/4\omega$  diagnostics respectively. The solid lines using Eq. 1 to find the frequency of the resonant ion-acoustic modes for the densities experimentally measured using Thomson scattering at different positions in the gas jet ( $n_e(r = 0\mu\text{m}) = 1.2 \times 10^{20} \text{ cm}^{-3}$ ,  $n_e(r = 350\mu\text{m}) = 7.0 \times 10^{19} \text{ cm}^{-3}$ ,  $n_e(r = 550\mu\text{m}) = 3.5 \times 10^{19} \text{ cm}^{-3}$ ,  $n_e(r = 700\mu\text{m}) = 2.5 \times 10^{19} \text{ cm}^{-3}$ ).

the Lawrence Livermore National Laboratory (Fig. 2). The nitrogen gas-jet plasmas were produced by two high-power ( $\lambda = 1054 \text{ nm}$ ) laser beams. The neutral gas density was well-characterized using a Mach-Zender interferometer. The heater beams were pointed through the center of the 1 mm diameter gas jet, 1.5 mm from the jet exit. The primary heater beam used 450 J in a 1.2 ns laser pulse. The beam was focused to a 1.2 mm diameter focal spot at the target chamber center (TCC) through a phase zone plate (PZP) using a f/6.7 lens producing plasmas with a range of electron temperatures ( $100 \text{ eV} < T_e < 650 \text{ eV}$ ) and densities ( $10^{19} \text{ cm}^{-3} < n_e < 10^{20} \text{ cm}^{-3}$ ). The second heater beam used 100 J in 1.2 ns, 0.3 ns after the falling edge of the primary heater beam (Fig. 2(b)). This beam was focused using a f/6.7 lens with a continuous phase plate (CPP) to a 200 micron diameter focal spot at the TCC.

Two 0.5 J Thomson-scattering probe lasers at two different wavelengths,  $\lambda_{ts}^{2\omega} = 532 \text{ nm}$  and  $\lambda_{ts}^{4\omega} = 266 \text{ nm}$ , were used to probe thermal ion-acoustic fluctuations with significantly different wave vectors. The  $2\omega$  and  $4\omega$  probe beams were focused using an f/5 and f/10 lens respectively to a diameter at the TCC of 75 microns. Through conservation of momentum, the ion-acoustic wave vector probed by each diagnostic ( $k_a$ ) is defined by the scattering geometry and the wavelength of the probe laser (Fig. 2(c)).

Two f/5 collection lenses collimated light scattered from a single Thomson-scattering volume in the plasma.

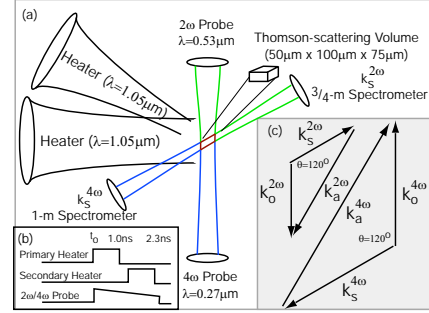


FIG. 2: (a) The experimental setup is shown., (b) Beam timing, (c) A k-vector diagram shows the ion-acoustic waves,  $k_a^{ts} \simeq 4\pi/\lambda_{ts} \sin \theta/2$ , that are probed.

The scattered light was then focused onto the slit of a 3/4-meter (for  $2\omega$ ) and a 1-meter (for  $4\omega$ ) imaging spectrometer using two f/10 focusing lenses. The optical configurations provided a magnification of two. The spectrometers were coupled to Hamamatsu streak cameras. The linear dispersion for the  $2\omega$  and  $4\omega$  Thomson-scattering diagnostics were  $0.0047 \text{ nm/pixel}$  and  $0.0012 \text{ nm/pixel}$  respectively. The instrument resolution was  $FWHM_{2\omega} = 12 \text{ pixels}$  ( $0.056 \text{ nm}$ ) and  $FWHM_{4\omega} = 18 \text{ pixels}$  ( $0.021 \text{ nm}$ ) defined by  $100\mu\text{m}$  slits on the entrance of the spectrometers.

The Thomson-scattering volume was defined in space using a 100 micron glass ball that was suspended  $\sim 3 \text{ mm}$  over the center of the gas jet. All beams were aligned to the ball at the TCC. The glass ball was back-lit and imaged through the  $2\omega$  and  $4\omega$  Thomson-scattering diagnostics. The ball was viewed through the streak camera in focus mode and both the spectrometer and the streak camera slits were closed to  $100\mu\text{m}$  and  $200\mu\text{m}$  respectively around the center of the ball. This defined a  $2\omega$  and a  $4\omega$  Thomson-scattering volume ( $50 \mu\text{m} \times 100 \mu\text{m} \times \sim 75\mu\text{m}$ ) located at the TCC. This alignment procedure resulted in a global positioning error between the gas jet and the overlapping Thomson-scattering volumes of 400 microns. To probe different locations within the plasma, the jet was moved using a micrometer which provided a relative accuracy better than 50 microns.

Figure 1 shows the dispersion of the ion-acoustic fluctuations for a range of densities measured using multiple Thomson-scattering diagnostics. Each set of points corresponds to the temporal evolution in the electron temperature on a single shot. The wavelength separation between the resonant spectral peaks for each Thomson-scattering diagnostic ( $\Delta\lambda_{ts}$ ), at various times (every 200ps), was determined using independent Gaussian fits to both sides of the Thomson-scattering spectra. In order to clearly observe the effects of the dispersion on the ion-acoustic fluctuations, the  $2\omega$  Thomson-scattering results were normalized by the ratio in wave vectors

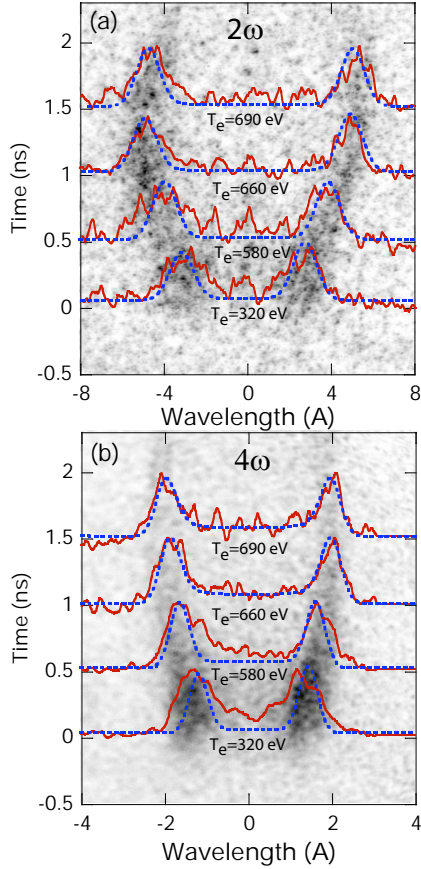


FIG. 3: Thomson scattering data from the same scattering volume in the gas-jet plasma observed with two different detectors measured the local ( $r = 350\mu\text{m}$ ) electron temperature as a function of time and the time average local density ( $n_e(r = 350\mu\text{m}) = 7 \times 10^{19} \text{cm}^{-3}$ ). The spectral profiles (solid-red line) are averaged over 200ps. The calculated theoretical form factor fit is shown for each time (dashed-blue line).

( $\frac{k_{4\omega}}{k_{2\omega}} = 2$ ), therefore, the difference between the normalized  $2\omega$  wavelength separation and the  $4\omega$  wavelength separation ( $\frac{\Delta\lambda_{2\omega}}{2} - \Delta\lambda_{4\omega}$ ) is zero for a non-dispersive plasma.

Figure 1(b) shows good agreement between the measured and calculated ion-acoustic frequencies over a large range of densities and temperatures. The measured frequencies for the ion-acoustic fluctuations were determined directly by the wavelength separation in the spectral peaks measured by Thomson scattering,  $\omega_a = \frac{\pi c}{\lambda_{ts}^2} \Delta\lambda_{ts}$ . The Debye length for each point was measured by simultaneously fitting the form factor (Eq. 1) to the  $2\omega$  and  $4\omega$  spectra; at each time, a single temperature was determined from both sets of data while a single density was determined using the peak tempera-

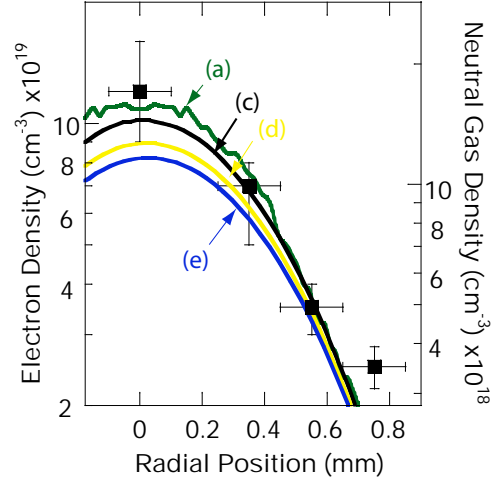


FIG. 4: (a) The 3-D neutral density profile (green curve) for the gas jet was measured using interferometry 1.5-mm above the gas jet (right axis). (b) Two Thomson-scattering diagnostics measured the electron density profile of the plasma (squares). Hydrodynamic simulations used the initial measured 3-D profile to calculate the electron density; (c)  $t=0.25\text{ns}$ , (d)  $t=0.5\text{ns}$ , (e)  $t=1.0\text{ns}$ .

ture fit where the system is most sensitive to electron density. Figure 3 shows a set of fits for a Thomson-scattering volume located at  $r = 350\mu\text{m}$ . The constant density curves in Fig. 1 were calculated by the theoretical form factor (Eq. 1), using the densities measured with Thomson scattering. Each curve corresponds to a single shot and a single density at a specific location defined by the Thomson-scattering volume. For these simulations a reasonable ion temperature was assumed ( $\frac{T_i}{T_e} = 0.3$ ); the main results of this paper are not sensitive to the ion temperature as long as  $T_i \ll T_e$ .

Simultaneously measuring two independent ion-acoustic frequencies provides a direct measure of the electron temperature and density. Using the results from Fig. 1, the density profile in the gas jet was measured and shows good agreement to the independent interferometer measurements (Fig. 4). The relative error in the position of the density measurement is shown by the error bars; there is a  $400\mu\text{m}$  uncertainty in the global position of the data set and the initial position of the gas jet. The density profiles are shown to vary by less than 20% over the time of the experiment using a hydrodynamic simulation performed with the code HYDRA (Fig. 4(c-d)) [5]. The HYDRA simulations used the experimental laser parameters and the 3-dimensional neutral gas density profile measured using interferometry as initial conditions.

The error bars shown for the measured density data in Fig. 4 were determined by the error in the measurement of both ion-acoustic frequencies using the high temper-

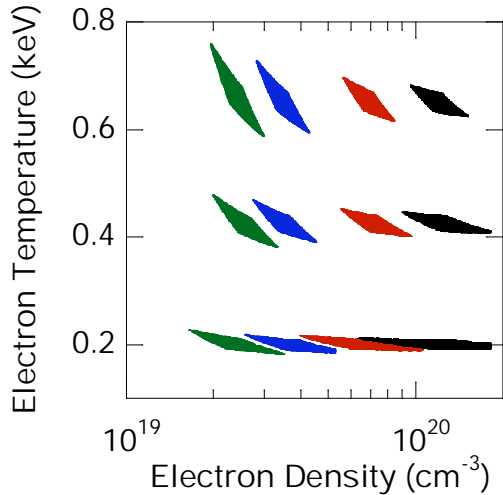


FIG. 5: Each region was calculated for the measured electron densities and temperatures using the actual measurement errors for each Thomson-scattering diagnostic. The error bars in Fig. 4 were determined using the extreme values in the calculated regions for each measured density at the peak electron temperature.

ature results where the diagnostic is most sensitive to density (larger absolute  $\Delta\lambda_{ts}$ ). Figure 5 shows a series of calculated regions defined by a location in parameter space ( $T_e$ ,  $n_e$ ) consistent with a given measurement of two ion-acoustic frequencies. The regions were calculated for the measured electron temperatures and electron densities shown in Fig. 4 using a constant error in the respective measurements of the wavelength separation ( $\delta\lambda_{4\omega} = 0.0014$  nm and  $\delta\lambda_{2\omega} = 0.005$  nm). When the electron temperature is low, the wavelength separation is small. If  $k\lambda_{de}$  is also low, the diagnostic is insensitive to density and the error in the density results are dominated by the error in the measurement of the ion-acoustic peaks (bottom right area in Fig. 5).

This technique is well suited for large laser facilities where other density diagnostics have not been successful in measuring local electron plasma density and temperature. Two ion-acoustic frequencies can be measured by either using two probe wavelengths or a single probe laser with two significantly different scattering angles. A small angle diagnostic ( $k_1$ ) can be chosen to provide a good measure of the electron temperature with a small dependence on the density ( $k_1\lambda_{de} < 1$ ) while a large an-

gle diagnostic ( $k_2$ ) would provide a good measure of the electron density ( $k_2\lambda_{de} > 1$ ). There is a limitation for large angles (for a given probe wavelength) given by the constraint of remaining in the collective Thomson scattering regime ( $\frac{ZT_e}{T_i} \gg k^2\lambda_{de}^2$ ) while there is a practical limit for small angles given by instruments ability to resolve the spectral peaks (i.e. the wavelength separation scales with the angle).

For a typical inertial confinement fusion plasma ( $T_e = 5$  keV,  $N_e = 5 \times 10^{20}$  W-cm $^{-3}$ ) the optimal scattering angles for the two collection optics are  $40^\circ < \theta_{k_2} < 80^\circ$  ( $0.4 < k_2\lambda_{de} < 0.7$ ) and  $\theta_{k_1} > 140^\circ$  ( $k_1\lambda_{de} > 0.9$ ); using these scattering angles, a single  $4\omega$  probe laser, and typical instrument resolutions, the local density could be measured to better than 25% with an electron temperature measurement to within 10%.

In summary, we have shown that the sound speed of ion-acoustic fluctuations are dependent on their frequency; this measure of the dispersion of ion-acoustic fluctuations is a verification of a fundamental plasma property in a dense high-temperature ICF plasma. The novel use of two Thomson-scattering diagnostics has allowed us to measure the local frequency of the ion-acoustic fluctuations at two significantly different wave vectors. We have further shown that this technique could be adapted to large ICF facilities to measure simultaneously the local electron temperature and density to high accuracy.

We would like to acknowledge the efforts of the Janus Laser Crew. We thank S. Dixit, M. Rushford, C. Hoaglan, and M. Aasen for the design and a fabrication of the CPP. Furthermore, we thank R. Griffith for the streak camera support. This work was performed under the auspices of the U.S. Department of Energy by the Lawrence Livermore National Laboratory under Contract No. W-7405-ENG-48.

\* Electronic address: [froula1@llnl.gov](mailto:froula1@llnl.gov)

† Also at Engineering Department, University of British Columbia.

‡ Also at Department of Applied Science, University of California at Davis.

- [1] S. H. Glenzer et al., Phys. Rev. Lett. **82**, 97 (1999).
- [2] J. A. Fejer, Can. J. Phys. **38**, 1114 (1960).
- [3] S. H. Glenzer et al., Physical Review E **55** (1997).
- [4] H. Tanaka et al., Phys. Rev. Lett. **16**, 1079 (1966).
- [5] M. Marinak et al., Phys. Plasmas **5**, 1125 (1998).